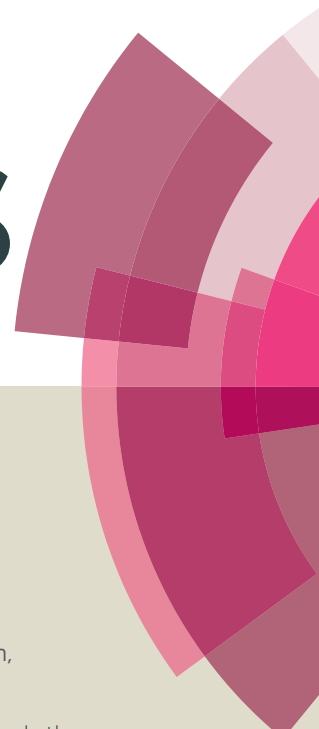


RSC Advances



This article can be cited before page numbers have been issued, to do this please use: P. Yang, H. Wen, C. Huang and Y. Zhu, *RSC Adv.*, 2016, DOI: 10.1039/C6RA15965F.



This is an *Accepted Manuscript*, which has been through the Royal Society of Chemistry peer review process and has been accepted for publication.

Accepted Manuscripts are published online shortly after acceptance, before technical editing, formatting and proof reading. Using this free service, authors can make their results available to the community, in citable form, before we publish the edited article. This *Accepted Manuscript* will be replaced by the edited, formatted and paginated article as soon as this is available.

You can find more information about *Accepted Manuscripts* in the [Information for Authors](#).

Please note that technical editing may introduce minor changes to the text and/or graphics, which may alter content. The journal's standard [Terms & Conditions](#) and the [Ethical guidelines](#) still apply. In no event shall the Royal Society of Chemistry be held responsible for any errors or omissions in this *Accepted Manuscript* or any consequences arising from the use of any information it contains.

**Synthesis and chemosensory properties of two-arm
truxene-functionalized conjugated polyfluorene containing
terpyridine moiety**

Po-Chih Yang*, Hua-Wen Wen, Chih-Wei Huang and Yi-Ning Zhu

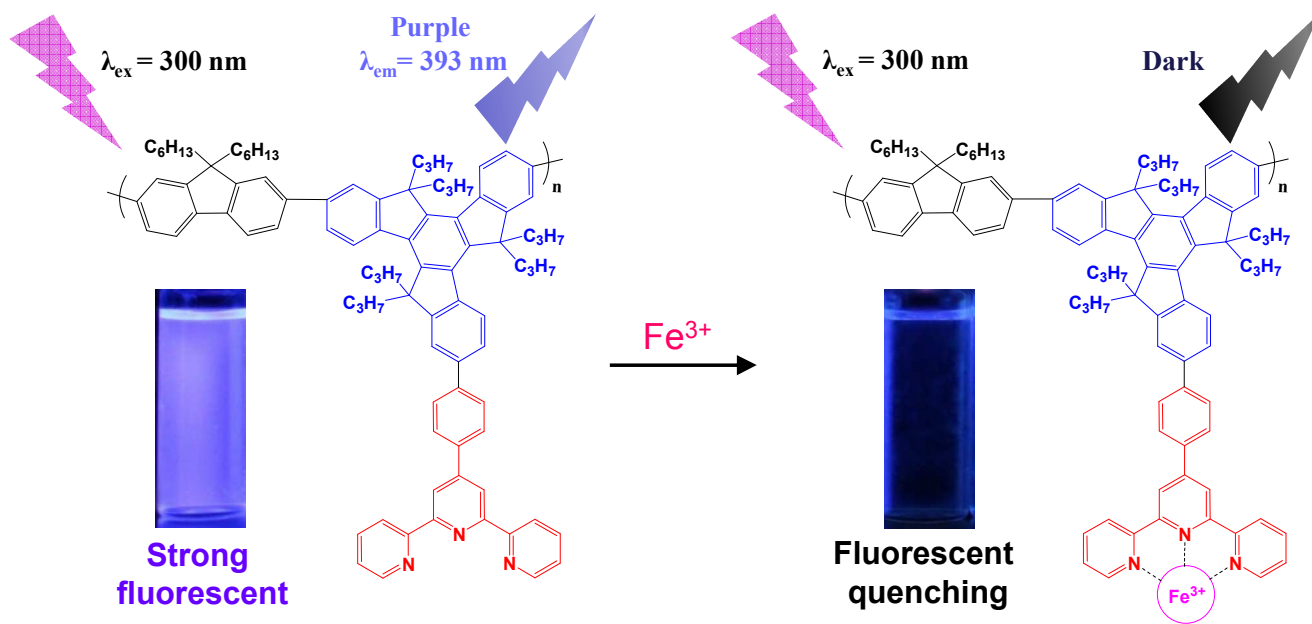
Department of Chemical Engineering and Materials Science, Yuan Ze University,

Chung-Li, Taoyuan City 32003, Taiwan

* Corresponding author. Tel.: +886 3 4638800; fax: +886 3 4559373.

E-mail address: pcyang@saturn.yzu.edu.tw (P.-C. Yang).

Graphical abstract



ABSTRACT

We report the responsive fluorescence chemosensory phenomena of a truxene-functionalized conjugated polymer (**P1**) with pendant terminal terpyridine (tpy) groups as receptors of metal ions synthesized through Suzuki polymerization. We examined the structural effect of tpy units on the sensory characteristics of fluorescent chemosensors. The weight-average molecular weight (M_w) of **P1** was 1.08×10^4 g/mol, with the corresponding polydispersity index being 2.25. **P1** exhibited high thermal stability with the thermal decomposition temperature being 334.6 °C at 5% polymer weight loss. Photoluminescence titrations demonstrated that **P1** exhibited high sensing ability to Fe^{3+} ions, with a Stern–Volmer constant of $1.14 \times 10^6 \text{ M}^{-1}$. The limit of detection of Fe^{3+} was estimated at $2.13 \times 10^{-7} \text{ M}$. The first stepwise association constant (K_{a1}) for the **P1**/ Fe^{3+} complex was $4.48 \times 10^5 \text{ M}^{-1}$. The fluorescence of the **P1** solution that was quenched by Fe^{3+} ions recovered on the addition of trace CN^- anions because of the considerably high stability constant of the CN^- – Fe^{3+} complex. Our results suggest that the synthesized polymer is a promising material for chemosensory applications.

Introduction

In recent decades, the development of conjugated polymers has attracted increasing attention, because of their use as highly sensitive fluorescent chemosensors for sensing various analytes, measuring pH, and detecting metal ions and biological species in environmental applications by applying color or fluorescence intensities.¹⁻⁸ Fluorescent chemosensors generally contain three components: (1) a receptor, which is a sorting or recognition site for selecting analytes reliably; (2) a fluorophore, the luminescent properties of which should be changed completely after being combined with the target substance; and (3) an appropriate linker, which couples the two parts.⁹ Fluorescent chemosensors offer several crucial advantages over low-molecular-weight compounds. For instance, the chemical signals that are converted into electronic or optical signals when these conjugated polymers bind with an analyte can be transformed and enhanced effectively.¹⁰ Additionally, the fluorophore of a conjugated polymer used as a fluorescent chemosensor is always bonded at the conjugated backbone, along which the excitons can diffuse easily, resulting in the fluorescence intensity and bathochromic or hypsochromic shifts of fluorescence wavelengths of these polymers changing more markedly.¹¹⁻¹⁵ To date, series of conjugated polymers have been synthesized to detect cations, anions, and pH by incorporating specific receptors in polymers such as alkyl ethers,¹⁶ crown ethers,¹⁷ quinolones,¹⁸ bipyridines,^{19,20} and terpyridines (tpys).^{21,22}

The 5*H*-diindeno[1,2-*a*:1',2'-*c*]fluorine (truxene) unit, a C_{3h} symmetric polycyclic polyarene with a rigid planar π -conjugated configuration, has gained considerable interest and been developed in the past decade as an optoelectronic functional template in the fields of organic light-emitting diodes, organic photovoltaics, transistors, and chemosensors.²³ The truxene core is particularly suitable as a scaffold because its extended π -delocalized system can cause a substantial shift in the absorption spectrum toward the visible region. Because of their $d\pi$ - $p\pi^*$ back-bonding of the metal ions to pyridines and a chelation effect useful for multinuclear supramolecular construction, 2,2';6',2''-tpy units have a high binding affinity toward transition-metal ions.^{24,25} These supramolecular complexes between the tpy ligands and metal ions

have been thoroughly investigated because of their relevant optical, electronic and magnetic properties.²⁶⁻²⁸ Many studies have investigated tpy units as recognition sites, and it has been widely demonstrated that the choice of ligands has a marked influence on the detection of metal ions in biological and environmental systems.^{29,30} Combining these fluorophores consisting of truxene and tpy units affords a new platform for developing metallodendrimers and star-shaped macromolecules. However, thus far, only a few studies have reported on these molecules, whose structures contain truxene and tpy units.³¹⁻³³ Pei et al.³¹ prepared a series of linear and star-shaped rigid conjugated tpy ligands containing truxene or fluorene as the core with various linkages through coupling reactions. Additionally, their findings on the involved photophysical properties indicates that these compounds emit strong blue fluorescence in solutions, thereby providing potential for materials such as the hosts for constructing novel functionalized metallic materials in examining energy and electron-transfer processes.

In this work, we used Suzuki coupling polymerization to synthesize a novel rigid linear truxene-functionalized conjugated copolymer with pendant tpy groups (**P1**). We examined the structural effect of the tpy groups on the sensory characteristics of fluorescent chemosensors. Although many studies have investigated conjugated polymers carrying tpy units as recognition sites,^{24,25} research on linear truxene-based conjugated polymers with tpy recognition units is lacking. In contrast to previous studies, our contributions differ in that **P1** benefits from the strong conjugation and luminescence properties of the asymmetric two-arm-substituted truxene monomer (**M1**) to yield enhanced sensing ability when mediated with metal ions. In this study, we found that **P1** demonstrated a highly selective response and rapid, sensitive recognition to Fe³⁺ with a marked fluorescence change from bright purple to dark in the THF-H₂O mixture. The Stern–Volmer constant (K_{sv}) and limit of detection (LOD) were 1.14×10^6 M⁻¹ and 2.13×10^{-7} M, respectively. In addition, the resulting **P1**-Fe³⁺ complex exhibited a markedly selective fluorescence restoration with cyanide ions (CN⁻), making this polymer a promising material for high-potential chemosensory applications.

Experimental

Materials

Synthetic routes for the truxene-based monomer and polymer are shown in Schemes 1 and 2. The terpyridine-functionalized compound 4'-(4-bromophenyl)-2,2':6',2''-terpyridine (**1**), and the truxene-functionalized compounds, 5*H*-diindeno[1,2-*a*:1',2'-*c*]fluorene (**3**) and 5,5,10,10,15,15-hexapropyl-10,15-dihydro-5*H*-diindeno[1,2-*a*:1',2'-*c*]fluorene (**4**) were synthesized following the processes reported previously.³⁴⁻³⁷ Tetrahydrofuran (THF) and toluene were purified and distilled from sodium prior. *N,N*-dimethylformamide (DMF) was dried with appropriate drying agents, calcium hydride or sodium, then distilled under reduced pressure and stored over 4 Å molecular sieves before use. 1-Bromopropane (Aldrich, 98.5%), 3-phenylpropionic acid (Acros, 99.0%), bromine (Acros, 99.8%), bis(pinacolato)diboron (B₂Pin₂) (Acros, 95.0%), Pd(dppf)₂Cl₂ (Alfa, 99.0%) and other reagents were purchased from commercial Chemical Co. and used without further purification.

Measurements

All new compounds were identified by NMR and elemental analysis (EA). NMR spectra were recorded on a Bruker AMX-500 (¹H NMR: 500 MHz, ¹³C NMR: 125 MHz) spectrometer with CDCl₃ as solvent, and chemical shifts (δ) were reported in ppm using tetramethylsilane (TMS) as an internal standard. Elemental analysis was performed on a Heraeus CHN-O rapid elemental analyzer. Fast Atom Bombardment mass spectra (FABMS) were obtained on a JEOL JMS-700 mass spectrometer. Weight-average molecular weight (*M_w*) and polydispersity index (PDI) of polymer were measured with a gel permeation chromatograph (GPC), model CR4A from Shimadzu, using tetrahydrofuran (THF) as an eluent and the rate of elution was 1.0 ml min⁻¹; the instrument was calibrated with polystyrene standards (1000–136000 g/mol). Thermal analysis was performed using a differential scanning calorimeter (Perkin Elmer DSC 7) at a scanning rate of 20 K/min under nitrogen atmosphere. Thermogravimetric analysis (TGA) was performed under nitrogen atmosphere at a

heating rate of 20 K/min using a Perkin Elmer TGA-7 thermal analyzer. UV-vis absorption spectra were measured with a Jasco V-670 spectrophotometer. Fluorescence properties were detected with an OBB Quattro II fluorescence spectrophotometer. Fluorescence quantum yield (Φ_{PL}) of **P1** in solution were estimated at room temperature with poly(9,9-dihexylfluorene) (PF) as the standard ($\Phi_{\text{PL}} = 1.0$). Cyclic voltammograms (CV) were recorded with a voltammetric analyzer (model CV-50W from BAS) at room temperature under nitrogen atmosphere with a scanning rate of 100 mV/s. The measuring cell comprised platinum wire as the working electrode, Ag/AgNO₃ electrode as the reference electrode, and platinum wire electrode as the auxiliary electrode. The electrodes were immersed in acetonitrile containing 0.1 M (n-Bu)₄NClO₄ as electrolyte. All the computational calculations were performed at B3LYP/6-31G* level using density functional theory (DFT) with Gaussian 09 program.³⁸

Synthesis of intermediates and monomer

Synthesis of 4'-(4-bromophenyl)-2,2':6',2''-terpyridine (1). Yield: 40.5%. $T_m = 162.0$ °C. ¹H-NMR (CDCl₃, 500 MHz): δ_{H} (ppm) = 7.49 (t, 2H), 7.80 (d, 2H), 7.92 (d, 2H), 8.01 (t, 2H), 8.75 (d, 4H), 8.81 (s, 2H). ¹³C NMR (CDCl₃, 125 MHz, δ in ppm): 118.7, 121.5, 123.5, 124.0, 129.0, 132.2, 137.1, 149.1, 156.0. FABMS (m/z) 388 M⁺.

Synthesis of 4'-(4-(4,4,5,5-tetramethyl-1,3,2-dioxaborolan-2-yl)phenyl)-2,2':6',2''-terpyridine (2). A mixture of **1** (0.39 g, 1.0 mmol), bis(pinacolato)diboron (B₂Pin₂) (0.30 g, 1.2 mmol), K₂CO₃ (0.69 g, 5.0 mmol), Pd(dppf)₂Cl₂ (43 mg, 0.070 mmol) and DMF (30 mL) was carefully degassed. The mixture was stirred for 24 h at 90 °C under N₂. Water (400 mL) was added, and the crude product was filtered and washed with water. After dried, the crude product was dissolved in chloroform, washed with a saturated solution of EDTA and purified by recrystallized from ethanol to afford **2** as a white solid (0.24 g, 55.2%). ¹H NMR (CDCl₃, 500 MHz): δ_{H} (ppm) = 1.36 (s, 12H), 7.34 (t, 2H, $J = 4.0$ Hz), 7.83-7.92 (m, 6H), 8.65 (d, 2H, $J = 8.0$ Hz), 8.70-8.74 (m, 4H). ¹³C NMR (CDCl₃, 125 MHz, δ in ppm): 21.5, 83.3, 118.7, 121.6, 123.5, 124.0, 129.1, 132.2, 137.2, 149.1, 156.1. FABMS (m/z) 435 M⁺.

Synthesis of 2-bromo-5,5,10,10,15,15-hexapropyl-10,15-dihydro-5H-diindeno[1,2-a:1',2'-c]fluorene (5). To a stirred solution of **4** (0.59 g, 1.0 mmol) in chloroform (20 mL), a solution of bromine (0.08 g, 0.5 mmol) in 10 mL of chloroform was added dropwise at room temperature. After 12 h, the mixture was washed with a saturated sodium thiosulfate solution and brine. After removal of the solvent, the crude product was purified by recrystallized from ethanol to afford **5** (30.2%). ¹H NMR (CDCl₃, 500 MHz): δ_H (ppm) = 0.51 (m, 30H), 2.00-2.11 (m, 6H), 2.73-2.94 (m, 6H), 7.36-7.42 (m, 5H), 7.44-7.51 (m, 3H), 8.32-8.40 (m, 3H). ¹³C NMR (CDCl₃, 125 MHz, δ in ppm): 14.6, 17.3, 39.3, 56.2, 121.2, 124.7, 125.7, 126.0, 126.4, 129.5, 130.1, 137.6, 138.4, 138.8, 140.3, 145.1, 154.0, 156.4. FABMS (*m/z*) 672 M⁺.

Synthesis of 4'-(4-(5,5,10,10,15,15-hexapropyl-10,15-dihydro-5H-diindeno[1,2-a:1',2'-c]fluoren-2-yl)phenyl)-2,2':6',2''-terpyridine (6). A mixture of **2** (0.87 g, 2.0 mmol), **5** (1.35 g, 2.0 mmol), tetrakis(triphenyl phosphine)palladium (Pd(PPh₃)₄) (69 mg, 0.06 mmol), K₂CO₃ (2M, 6 mL) and toluene (20 mL) was carefully degassed. The mixture was stirred for 12 h at 90 °C under N₂. After removal of the solvent, the crude product was purified by recrystallized from ethanol/CH₂Cl₂ (1:5, v/v) to give **6** as a white solid (1.14 g, 63.2%). ¹H NMR (CDCl₃, 500 MHz): δ_H (ppm) = 0.50 (m, 30H), 1.92-2.23 (m, 6H), 2.65-3.00 (m, 6H), 7.16-7.61 (m, 11H), 7.67-7.91 (m, 6H), 8.03-8.22 (m, 2H), 8.59 (s, 2H), 8.61-8.76 (d, 4H). ¹³C NMR (CDCl₃, 125 MHz, δ in ppm): 14.7, 17.7, 38.3, 46.4, 118.1, 120.9, 124.2, 125.9, 126.8, 127.9, 128.4, 130.5, 134.9, 135.9, 137.0, 139.9, 140.8, 141.1, 147.8, 148.3, 149.2, 152.1, 155.4, 156.1. FABMS (*m/z*) 901 M⁺.

Synthesis of 4'-(4-(7,12-dibromo-5,5,10,10,15,15-hexapropyl-10,15-dihydro-5H-diindeno[1,2-a:1',2'-c]fluoren-2-yl)phenyl)-2,2':6',2''-terpyridine (M1). To a stirred solution of **6** (0.45 g, 0.5 mmol) in chloroform (15 mL), a solution of bromine (0.32 g, 2.0 mmol) in 10 mL of chloroform was added dropwise at room temperature. After 12 h, the mixture was washed with a saturated sodium thiosulfate solution and brine. Removal of the solvent gave a yellow solid. Recrystallization from ethanol/CH₂Cl₂ (1:5, v/v) afforded a white solid (0.18 g, 34.0%). *T*_m = 168.6 °C. ¹H NMR (CDCl₃, 500 MHz): δ_H (ppm) = 0.43-0.56 (m, 30H), 1.92-2.12 (m, 6H),

2.65-2.89 (m, 6H), 7.26-7.61 (m, 11H), 7.84-8.19 (m, 6H), 8.60 (s, 2H), 8.62-8.76 (d, 4H). Anal. Calcd. (%) for $C_{66}H_{65}Br_2N_3$: C, 74.78; H, 6.18; N, 3.96. Found: C, 74.92; H, 6.22; N, 4.01. ^{13}C NMR ($CDCl_3$, 125 MHz, δ in ppm): 14.7, 17.6, 38.3, 46.4, 118.1, 120.9, 124.1, 125.9, 126.8, 127.9, 130.5, 134.9, 135.9, 137.1, 139.9, 140.7, 141.1, 147.8, 148.3, 149.2, 152.1, 155.4, 156.1. Anal. Calcd. (%) for $C_{66}H_{65}Br_2N_3$: C, 74.78; H, 6.18; N, 3.96. Found: C, 74.84; H, 6.09; N, 4.01. FABMS (m/z) 1060 M^+ .

Synthesis of conjugated polymer

Synthesis of poly[2,7-(5,5,10,10,15,15-hexapropyl-10,15-dihydro-5H-diindeno[1,2-a:1',2'-c]fluorene)-alt-4'-phenyl-2,2':6',2''-terpyridine] (P1). The conjugated polymer **P1** was prepared using palladium-catalyzed Suzuki coupling reactions of monomers **A/M1** in toluene at 90 °C using $Pd(PPh_3)_4$ as the catalyst. A mixture of **A** (0.29 g, 0.5 mmol), **M1** (0.53 g, 0.5 mmol), $Pd(PPh_3)_4$ (49 mg, 0.04 mmol), K_2CO_3 (2M, 2 mL) and toluene (7 mL) was carefully degassed. The mixture was stirred for 72 h at 90 °C under N_2 . Then, bromobenzene (0.08 g, 0.5 mmol) and phenylboronic acid (0.06 g, 0.5 mmol) were added for the end capping by refluxing subsequently for 6 h each. The mixture was cooled to room temperature. After removal of the solvent, the residue was filtered in CH_3OH (500 mL) to precipitate out the polymer. The resulting precipitate was placed in a Soxhlet apparatus and extracted with refluxed CH_3OH for 72 h and then was dried in vacuum to give 0.23 g (44.3%). $M_w = 1.08 \times 10^4$ g/mol, PDI = 2.25. 1H NMR ($CDCl_3$, 500 MHz): δ_H (ppm) = 0.35-0.98 (br, CH_3 and CH_2), 1.76-2.44 (br, CH_2), 2.69-3.12 (br, CH_2), 7.27-9.10 (br, Ar-H). Anal. Calcd. (%) from feed ($C_{25}H_{32}$)($C_{66}H_{65}N_3$): C, 76.31; H, 6.78; N, 2.94. Found: C, 75.84; H, 6.54; N, 2.82.

Fluorescent titration with metal ions

Fluorescent titration experiments were performed in THF solutions. Stock solutions (1.0×10^{-3} M) of the chloride or nitrate salts of Ag^+ , Al^{3+} , Ba^{2+} , Ca^{2+} , Fe^{2+} , Fe^{3+} , K^+ , Mg^{2+} , Mn^{2+} , Ni^{2+} , Pb^{2+} , Li^+ , and Zn^{2+} in deionized water were prepared. Titrations were performed by adding separately stock solutions to a test tube containing polymer

solution. All optical measurements were conducted immediately after the test solutions were prepared and thoroughly mixed. The final concentration of the polymer was 1.0×10^{-6} M. The percentage of water in THF was approximately 1.0%. The Stern–Volmer constant (K_{sv}) was estimated according to following equation:

$$(I_0/I) = 1 + K_{sv} [Q] \quad (1)$$

where I_0 and I are the intensities of PL spectra without and with a quencher, respectively, K_{sv} is the Stern–Volmer constant (quenching coefficient), and $[Q]$ is the concentration of the quencher ions. The stabilization of **P1**-Fe³⁺ complex (1.0×10^{-6} M in THF) was studied in the presence of some anions, including F⁻, Cl⁻, Br⁻, NO₃⁻, SO₄²⁻, S²⁻, and CN⁻ (2.0×10^{-5} M). The limit of detection (LOD) of **P1** was calculated on the basis of fluorescence titrations. To obtain the slope, the fluorescence emission at 393 nm was plotted as a concentration of Fe³⁺. The LOD was calculated using the following equation:

$$\text{Limit of detection (LOD)} = 3\sigma/S \quad (2)$$

where σ is the standard deviation of the blank signal, and S is the slope between the fluorescence intensity *versus* [Fe³⁺].

Results and Discussion

Synthesis of intermediates and monomer

Scheme 1 outlines the synthetic routes of the tpy-functionalized monomer **M1**. The bromo-functionalized compound **5**, 2-bromo-5,5,10,10,15,15-hexapropyl-10,15-dihydro-5*H*-diindeno[1,2-a:1',2'-c]fluorene, was prepared through the bromination reaction of compound **4** (5,5,10,10,15,15-hexapropyl-10,15-dihydro-5*H*-diindeno[1,2-a:1',2'-c]fluorene) with bromine at room temperature. The crude product was purified by recrystallized from ethanol to afford **5**, thus creating compound **5** with a yield of 30.2%. We prepared 4'-(4-(5,5,10,10,15,15-hexapropyl-10,15-dihydro-5*H*-diindeno[1,2-a:1',2'-c]fluoren-2-yl)phenyl)-2,2':6',2''-terpyridine (**6**) in a 63.2% yield by using the Suzuki coupling reaction of 4'-(4-(4,4,5,5-tetramethyl-1,3,2-dioxaborolan-2-yl)phenyl)-2,2':6',2''-terpyridine (**2**) with compound **5** in the presence of potassium carbonate at

90 °C. The reaction was performed using Pd(PPh₃)₄ as the catalyst. The target monomer, 4'-(4-(7,12-dibromo-5,5,10,10,15,15-hexapropyl-10,15-dihydro-5*H*-diindeno[1,2-*a*:1',2'-*c*]fluoren-2-yl)phenyl)-2,2':6',2''-terpyridine (**M1**), was prepared in a procedure similar to that for compound **5**, except that compound **6** was used instead of compound **4**, resulting in **M1** in a 34.0% yield. The chemical structures and constitutional composition of the synthesized monomer were confirmed using proton nuclear magnetic resonance (¹H NMR) spectroscopy. Fig. S1a shows the ¹H NMR spectrum of **M1** and the corresponding structural assignments. The characteristic chemical shifts of $\delta = 8.62\text{-}8.76$ (H_a) and $\delta = 8.60$ ppm (H_b) were attributed to the terpyridyl doublet and singlet proton signals in **M1**, respectively, and those of $\delta = 2.65\text{-}2.89$, $1.92\text{-}2.12$ and $0.43\text{-}0.56$ ppm were ascribed to the aliphatic methylene (H_c and H_d) and methyl (H_e) groups of the truxene unit, respectively. ¹³C NMR measurements (Fig. S2) were adapted to confirm the structure of the intermediates **1** and **5**. Fig. S3 and Fig. S4 show the FABMS (Fast Atom Bombardment Mass Spectroscopy) mass spectra of two representative tpy-functionalized intermediate **1** and monomer **M1**, respectively. In addition, the chemical structures of the synthesized monomer were also confirmed using elemental analysis.

Scheme 1

Synthesis and thermal properties of polymer

P1 was successfully synthesized from **M1** and **A** through a palladium-mediated Suzuki coupling reaction (Scheme 2). Fig. S1b shows the ¹H NMR spectrum of **P1** in CDCl₃. The ¹H NMR spectrum of **P1** exhibited peaks at approximately 8.97-9.10 ppm, which were assigned to shifts to the ortho and meta positions labeled H_a of the pyridine unit, whereas the protons (H_b) were the two aromatic protons of the 2,2':6',2''-terpyridyl segment at 8.82-8.96 ppm. The other aromatic protons appeared at 7.27-8.54 ppm. Finally, the ¹H NMR spectrum of **P1** had the alkyl group peaks at approximately 2.69-3.12, 1.94-2.38, 0.78-0.95 and 0.40-0.66 ppm assigned to the aliphatic protons labeled H_c, H_{d+e}, H_f, and H_{g+th}. The weight-average molecular weight

(M_w) of **P1** was 1.08×10^4 g mol⁻¹ with a corresponding polydispersity index of 2.25 (Table 1). The molar percentage of the tpy-functionalized monomer (**M1**) in **P1** was estimated at approximately 44.5% according to the integrated peak areas of the aliphatic group of truxene (H_c and H_d) and the methylene protons of fluorene (H_e). The estimated molar percentage of **M1** in the polymer was lower than that of the feed (50.0%), indicating that the lower percentage was attributed to the steric effect and electron-deficient character of the tpy monomer, resulting in reduced monomer reactivity. **P1** exhibited high thermal stability with the thermal decomposition temperature (T_d) being 334.6 °C at 5% polymer weight loss (Fig. 1). The residual weight of **P1** at 800 °C was approximately 61.2%, indicating high thermal stability.

Scheme 2, Figure 1, Table 1

Optical and electrochemical properties

Fig. 2 shows the absorption and PL spectra of **P1** in THF (1.0×10^{-6} M) and in thin films spin-coated from THF solutions (10 mg/mL) with the corresponding data summarized in Table 2. In THF, **P1** exhibited the main absorption peaks at 284 and 309 nm, which resulted from a π - π^* transition of the truxene units, consistent with a finding reported in the literature.³⁹ Another weak transition shoulder in **P1** was observed at approximately 363 nm, which was attributed to the intramolecular charge transfer (ICT) between the truxene donor groups and the tpy acceptor, leading to the observed ICT interaction and bathochromic shift.^{40,41} In the film state, the absorption maximum of **P1** was red-shifted (ca. 53 nm) relative to the solution state, resulting from aggregation caused by intra-chain or interchain interactions. The fluorescence maximum of **P1** in THF was 393 nm. In the film state, the emission maximum was situated at 433 nm, implying that excimers or exciplexes form in the film state. Table 2 lists the Stokes shift of **P1** at 96 nm, and the large shift may result from structural differences between the ground and excited states as well as migrated excitons in the segments of the chain, where the ring rotates more flexibly.

Fig. S5 depicts the estimated cyclic voltammogram of **P1** in CH₂Cl₂ at a scanning rate of 100 mV/s, and Table 3 presents a summary of the electrochemical data. The

highest occupied molecular orbital (HOMO) and lowest unoccupied molecular orbital (LUMO) energy levels were evaluated according to the equations $E_{\text{HOMO}} = -(E_{\text{ox}} + 4.8)$ eV and $E_{\text{LUMO}} = E_{\text{HOMO}} + E_{\text{g}}^{\text{opt}}$, where E_{ox} is the onset oxidation potential regarding the standard ferrocene/ferrocenium (FOC) redox system. The optical band gap ($E_{\text{g}}^{\text{opt}}$) was determined based on the onset absorption wavelength. The onset oxidation peaks of **P1** were observed at approximately 0.27 and 0.55 V. We attributed these two oxidation potentials of **P1** to the charge delocalization of extended π -systems of the truxene and fluorene groups, respectively. The estimated molecular orbital levels of **P1** are $-5.07/-5.35$ (HOMO/HOMO-1) and -2.06 eV (LUMO). The optical bandgap ($E_{\text{g}}^{\text{opt}}$) value for **P1**, determined according to the onset of absorption in the solution state, was 3.01 eV (412 nm).

Figure 2, Table 2, Table 3

Theoretical calculations

To obtain further insight into the electronic effect of polymer on the molecular geometry and electronic structure, density functional theory (DFT) calculations were performed using the B3LYP/6-31G* method to predict the minimum-energy conformations and the frontier molecular orbitals of the model compounds of **P1**. As presented in Fig. S6, the optimized structures of the model compound (i.e., repeating unit $n = 1$ in Scheme 2) revealed that the HOMO for **P1** is nearly delocalized on the whole backbone of the model compound, whereas the LUMO is mainly located on the tpy unit, indicating the efficient charge separation of the model compound. According to DFT calculations, the HOMO and LUMO values of **P1** were -5.49 and -1.52 eV, respectively. This also means that the theoretical bandgap ($E_{\text{g}}^{\text{the}}$) value for **P1** was 3.97 eV. This result was different from the data of the UV-vis absorption and CV experiments (i.e., $E_{\text{g}}^{\text{opt}} = 3.01$ eV), for which we attributed the larger bandgap to the small repeating unit number (i.e., $n = 1$) of the model compound. Additionally, we found that the model compound exhibited high coplanar arrangement, in which the largest dihedral angle was only 36.8° between truxene and tpy units, indicating that the efficient conjugation effect between truxene and tpy units was induced and leads

to the effective ICT.

Ion sensing properties

The tpy groups are generally employed as ligands to combine metal cations for generating complexes. Fig. 3a shows the effect of complexation with various metal ions (Ag^+ , Al^{3+} , Ba^{2+} , Ca^{2+} , Fe^{2+} , Fe^{3+} , K^+ , Mg^{2+} , Mn^{2+} , Ni^{2+} , Pb^{2+} , Li^+ , and Zn^{2+}) on the fluorescence spectra of **P1** in THF- H_2O solution. The fluorescence intensity of the **P1** solution decreased significantly on the addition of Fe^{2+} , Fe^{3+} , Ag^+ , Zn^{2+} , or Ni^{2+} ions (Fig. 3a), indicating that the tpy chelating moiety in the side chain effectively transferred energy from the conjugated polymer backbone to these cations, thus leading to the fluorescence quenching of **P1**. In particular, **P1** was quenched completely by Fe^{3+} ions with an ion concentration of 5.0×10^{-5} M, indicating their high selectivity toward this cation. The quenching mechanism of polymer can be attributed to the photoinduced energy transfer occurring in a collision (dynamic quenching) between the excited fluorophore and metal ions. We also attributed the quenching behavior to strong cation binding between Fe^{3+} ions and the tpy chelating groups; the binding results from the effective energy transfer migration between the receptors and polymer chains. Thus, **P1** can be used in polymer chemosensors for detecting metal ions.

Fig. 3b shows the photoluminescence response profiles (i.e., I_0/I) of **P1** in the presence of various metal ions with an ion concentration of 5.0×10^{-5} M. The emission colors of fluorescence responses to various metal ions were visible (Fig. 3d). We found that **P1** showed high sensitivity toward Fe^{3+} with a marked fluorescence change from bright purple to dark in the THF- H_2O mixture. These results indicated that the shorter diameter (1.28 Å) and higher charge (1.83) of Fe^{3+} might lead to a higher electron-accepting capability and consequently more stable complexes. Moreover, these two factors (i.e., diameter and charge) might play a vital role in determining the coordination strength of Fe^{3+} ions accompanying tpy units.⁴² The five electrons (Fe^{3+} : d^5 electron configuration) may be present as two orbitals occupied by pairs of electrons and one having single occupancy, leading to the inner-orbital complex, which was more stable than the other host/metal complexes.⁴³ The Φ_{PL} value of **P1** in

the presence of Fe^{3+} ions decreased by approximately 99.8% (i.e., from 1.82 to 0.6×10^{-2}). Moreover, adding Zn^{2+} ions induced a broad red-shifted emission in the range of 500-600 nm for **P1**, which was ascribed to the enhancement of the ICT processes. Adding metal ions (Ag^+ , Al^{3+} , Ca^{2+} , Fe^{2+} , Fe^{3+} , K^+ , Mg^{2+} , Ni^{2+} , and Li^+) into **P1** led to a new emission peak at approximately 601 nm, which is attributable to the phosphorescence derived from the **P1**-metal ion complexes.⁴⁴⁻⁴⁶ These results also indicated that these shifts were ascribed to the similar energy level of metal ions and truxene triplets and to the spin-orbit coupling induced by the metal ions,⁴⁵ or to the formation of the polymeric self-assembled structure by the metal ion coordination, which hinders intramolecular rotations and motions of the core chromophore and favors radiative deactivation of the luminescent excited state.⁴⁶

Figure 3a, Figure 3b, Figure 3c, Figure 3d

To quantitatively evaluate the fluorescence quenching attained by adding Fe^{3+} , the fluorescence spectra and the response of **P1** to titration with Fe^{3+} were studied in THF. The emission intensities at 393 nm (i.e., $I_{393\text{ nm}}$) gradually decreased with increasing Fe^{3+} concentrations (Fig. 4a). The slope of the Stern–Volmer plot turned noticeably upward (i.e., static quenching), resulting from strong tpy chelation to the transition metal ions, when Fe^{3+} concentrations were greater than 2.0×10^{-5} M. K_{sv} for **P1** in the presence of low Fe^{3+} concentrations (below approximately 1.5×10^{-5} M) was 1.14×10^6 M^{-1} . The estimated detection limit for **P1** toward Fe^{3+} was as low as 2.13×10^{-7} M, enabling **P1** to be a selective and sensitive Fe^{3+} probe. As shown in Fig. 3b, a new absorption peak at 580 nm appeared in **P1** solution when it was titrated with Fe^{3+} ions. The color of **P1** solution under sunlight changed from colorless to purple (Fig. 3c), suggesting that **P1** can be employed as a useful probe for detecting Fe^{3+} ions. The first stepwise association constant (K_{a1}) for the **P1**– Fe^{3+} complex was calculated following the photoluminescence titration experiment.^{47,48} The K_{a1} of this system for **P1** was 4.48×10^5 M^{-1} at 393 nm (Fig. 4a).

Figure 4a, Figure 4b

Fig. 5 shows the specificity of **P1** (1.0×10^{-6} M in THF) toward Fe^{3+} ions with various cations (1.0×10^{-5} M in water). We examined whether **P1** can retain the sensing

response to Fe^{3+} in the presence of the competitive cations. The changes in the enhanced ratio of fluorescence intensity (i.e., I_0/I) of polymer were measured on the addition of other metal ions. No responses were found, as shown by the black bars in this figure. Adding 1.0×10^{-5} M of Fe^{3+} in **P1** solutions then yielded 160- to 310-fold emission enhancements with and without other metal ions, respectively (Fig. 5, red bars). In other words, the presence of other metal ions seemed to have no effect on the response of **P1** toward Fe^{3+} . Therefore, the fluorescence interference titration indicated that the Fe^{3+} -dependent fluorescence response of **P1** was not affected by other transition metal ions.

Figure 5

To determine whether the **P1**- Fe^{3+} complex can be used as an anion selective probe, the response of the complex toward anions (F^- , Cl^- , Br^- , NO_3^- , SO_4^{2-} , S^{2-} , and CN^-) was investigated (Fig. 6a). The fluorescence response profiles (i.e., I/I_0) of **P1**- Fe^{3+} complexes in the presence of CN^- anions with a concentration of 2.0×10^{-5} M are provided in Fig. 6b. These data illustrate that the fluorescence intensity of the **P1**- Fe^{3+} complex increased considerably on the addition of CN^- ions, whereas complexation with other anions induced no obvious shift in the emission peak because of the poor coordination of Fe^{3+} with these anions. However, in the presence of S^{2-} , the PL spectrum of the **P1**- Fe^{3+} complex exhibited a slight increase in the fluorescence intensity. The complex demonstrated a markedly selective fluorescence “turn-on” behavior exclusively with CN^- ions, indicating that CN^- ions could effectively coordinate with Fe^{3+} instead of **P1**. This finding is attributed to the high stability of the Fe^{3+} - CN^- complex.^{49,50} Hence, the fluorescence intensities of **P1** could be revived by the transformation from the polymer- Fe^{3+} complex (quenched) to the free polymer (revived). When the concentration of added CN^- was 1.8×10^{-5} M, the fluorescence intensity recovered by up to 48.6% of the original intensity, whereas adding S^{2-} led to a recovery of up to 6.5% of the original intensity (Fig. 7). In addition, addition of other anions induced a recovery of approximately 0.1% of the original intensity, enabling **P1** to be used as a sensitive CN^- sensor.

Figure 6a, Figure 6b, Figure 7

Conclusions

In summary, a new truxene-functionalized conjugated copolymer with tpy groups as receptors (**P1**) was synthesized, and its corresponding optical and sensory characteristics were evaluated. **P1** exhibited high thermal stability with the thermal decomposition temperature being 334.6 °C at 5% weight loss. **P1** exhibited high sensitivity toward Fe³⁺ ions (“turn-off”) with a Stern–Volmer constant (K_{sv}) of $1.14 \times 10^6 \text{ M}^{-1}$ and an LOD of $2.13 \times 10^{-7} \text{ M}$. Furthermore, the polymer-Fe³⁺ complex demonstrated particularly selective fluorescence restoration (“turn-on”) abilities with CN⁻ ions. These results indicate that **P1** can meet the selective requirements for environmental applications and be sufficiently sensitive to detect Fe³⁺ ions in environmental water samples, including drinking water.

Acknowledgements

Financial support for this work by grants from the Ministry of Science and Technology, Taiwan (Nos. 103-2221-E-155-072 and 105-2221-E-155-079) is gratefully appreciated.

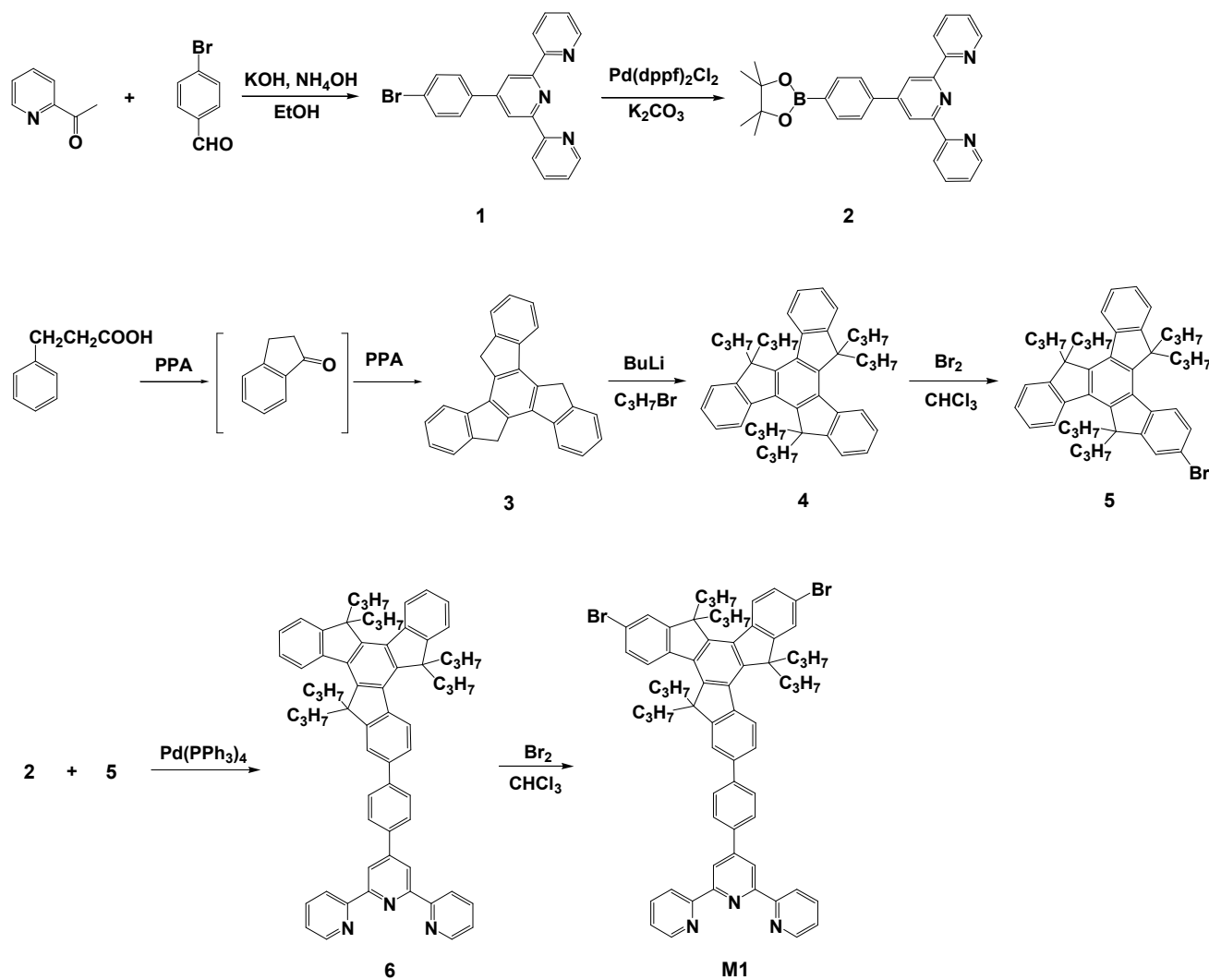
Notes and references

- 1 P. G. Del Rosso, M. J. Romagnoli, M. F. Almassio and C. A. Barbero, *Sens. Actuators B*, 2014, 203, 612–620.
- 2 Y. Yang, G. Zhang, H. Luo, J. Yao, Z. Liu and D. Zhang, *ACS Appl. Mater. Interfaces*, DOI: 10.1021/acsami.5b08078, 2015.
- 3 Y. Zhou, L. Tang, G. Zeng, C. Zhang, Y. Zhang and X. Xie, *Sens. Actuators B*, 2016, 223, 280–294.
- 4 O. S. Wolfbeis, *Chem. Soc. Rev.*, 2015, 44, 4743–4768.
- 5 M. Saleem and K. H. Lee, *RSC Adv.*, 2015, 5, 72150–72287.
- 6 S. Cao, Z. Pei, Y. Xu, R. Zhang and Y. Pei, *RSC Adv.*, 2015, 5, 45888–45896.
- 7 L. Zhang, X. Lou, Y. Yu, J. Qin and Z. Li, *Macromolecules*, 2011, 44, 5186–5193.
- 8 X. Lou, Y. Zhang, S. Li, D. Ou, Z. Wan, J. Qin and Z. Li, *Polym. Chem.*, 2012, 3,

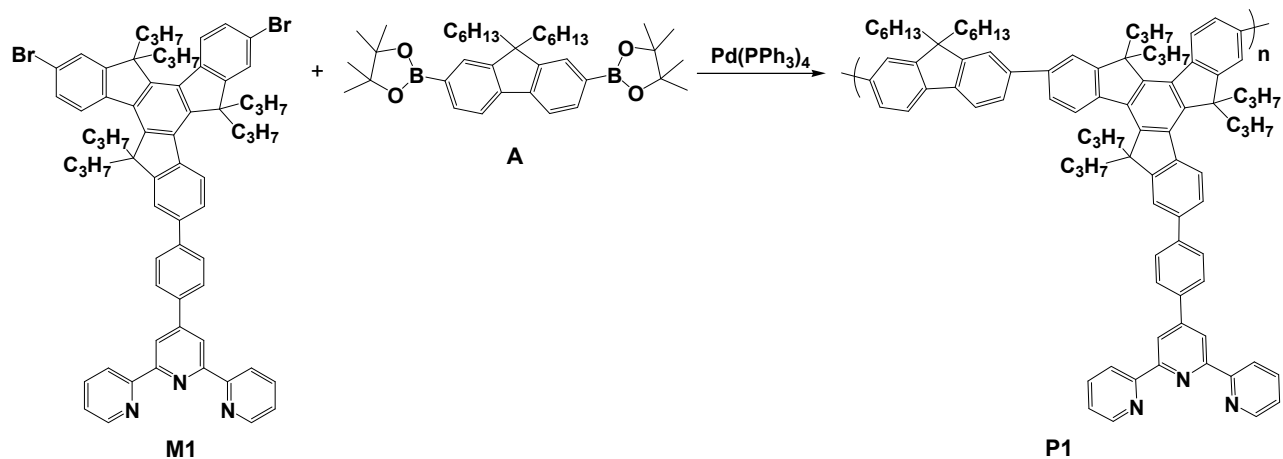
- 1446–1452.
- 9 Y. Long, H. Chen, H. Wang, Z. Peng, Y. Yang, G. Zhang, N. Li, F. Liu and J. Pei, *Anal. Chim. Acta.*, 2012, *744*, 82–91.
- 10 Z. Chen, Q. Wang, X. Wu, Z. Li and Y. B. Jiang, *Chem. Soc. Rev.*, 2015, *44*, 4249–4263.
- 11 C.M. Darr, V. Korampally, B. Chen, K. Gangopadhyay, S. Gangopadhyay, *Sens. Actuators B*, 2014, *202*, 1088–1096.
- 12 A. C. Bhasikuttan and J. Mohanty, *Chem. Commun.*, 2015, *51*, 7581–7597.
- 13 L. Qin, B. Lu, J. Xu, G. Zhang and S. Zhang, *RSC Adv.*, 2014, *4*, 28368–28376.
- 14 C. Kaewtong, N. Niamsa, B. Pulpoka and T. Tuntulani, *RSC Adv.*, 2014, *4*, 52235–52240.
- 15 D. Mao, X. Liu, Q. Qiao, W. Yin, M. Zhao, J. M. Cole, J. Cui and Z. Xu, *Analyst*, 2015, *140*, 1008–1013.
- 16 A. Balamurugan, V. Kumar and M. Jayakannan, *Chem. Commun.*, 2014, *50*, 842–845.
- 17 G. Xiang, L. Wang, W. Cui, X. An and L. Zhou, *Sens. Actuators B*, 2014, *196*, 495–503.
- 18 H. Kim, G. R. You, G. J. Park, J. Y. Choi, I. Noh, Y. Kim, S. J. Kim, C. Kim and R. G. Harrison, *Dyes Pigm.*, 2015, *113*, 723–729.
- 19 F. Jin, W. Shu, X. Yu, Y. Zhang, L. Sun, Y. Liu, D. Tao, H. Zhou and Y. Tian, *Dyes Pigm.*, 2015, *121*, 379–384.
- 20 A. Bellusci, M. Ghedini, L. Giorgini, F. Gozzo, E. I. Szerb, A. Crispini and D. Pucci, *Dalton Trans.*, 2009, 7381–7389.
- 21 S. Jing, C. Zheng, S. Pu, C. Fan and G. Liu, *Dyes Pigm.*, 2014, *107*, 38–44.
- 22 Z. B. Zheng, S. Y. Kang, Y. Zhao, N. Zhang, X. Yi and K. Z. Wang, *Sens. Actuators B*, 2015, *221*, 614–624.
- 23 F. Goubard, and F. Dumur, *RSC Adv.*, 2015, *5*, 3521–3551.
- 24 M. Zheng, H. Tao, Z. Xie, L. Zhang, X. Jing and Z. Sun, *ACS Appl. Mater. Interfaces*, 2013, *5*, 1078–1083.
- 25 S. Karmakar, D. Maity, S. Mardanya and S. Baitalik, *Dalton Trans.*, 2015, *44*,

- 18607–18623.
- 26 U. S. Schubert, H. Hofmeier and G. R. Newkome, *Modern Terpyridine Chemistry*, Wiley-VCH, Weinheim, Germany, 2006.
- 27 A. Wild, A. Winter, F. Schlütter and U. S. Schubert, *Chem. Soc. Rev.*, 2011, *40*, 1459–1511.
- 28 E. C. Constable, *Chem. Soc. Rev.*, 2007, *36*, 246–253.
- 29 P. Mahato, S. Saha, P. Das, H. Agarwalla and A. Das, *RSC Adv.*, 2014, *4*, 36140–36174.
- 30 Y. Zhou and J. Yoon, *Chem. Soc. Rev.*, 2012, *41*, 52–67.
- 31 S. C. Yuan, H. B. Chen, Y. Zhang and J. Pei, *Org. Lett.*, 2006, *8*, 5701–5704.
- 32 B. Ventura, A. F. Barigelletti, S. Diring and R. Ziessel, *Inorg. Chem.*, 2010, *49*, 8333–8346.
- 33 J. L. Wang, Y. T. Chan, C. N. Moorefield, J. Pei, D. A. Modarelli, N. C. Romano and G. R. Newkome, *Macromol. Rapid Commun.*, 2010, *31*, 850–855.
- 34 S. K. Lee, D. H. Hwang, B. L. Jung, N. S. Cho, J. Lee, J. D. Lee and H. K. Shim, *Adv. Funct. Mater.*, 2005, *15*, 1647–1655.
- 35 F. Dumur, C. R. Mayer, E. Dumas, F. Miomandre, M. Frigoli and F. Sécheresse, *Org. Lett.*, 2008, *10*, 321–324.
- 36 X. Y. Cao, H. Zi, W. Zhang, H. Lu and J. Pei, *J. Org. Chem.*, 2005, *70*, 3645–3653.
- 37 J. Pei, J. L. Wang, X. Y. Cao, X. H. Zhou and W. B. Zhang, *J. Am. Chem. Soc.*, 2003, *125*, 9944–9945.
- 38 Gaussian 09, Revision A.1, M. J. Frisch, G. W. Trucks, H. B. Schlegel, G. E. Scuseria, M. A. Robb, J. R. Cheeseman, G. Scalmani, V. Barone, B. Mennucci, G. A. Petersson, H. Nakatsuji, M. Caricato, X. Li, H. P. Hratchian, A. F. Izmaylov, J. Bloino, G. Zheng, J. L. Sonnenberg, M. Hada, M. Ehara, K. Toyota, R. Fukuda, J. Hasegawa, M. Ishida, T. Nakajima, Y. Honda, O. Kitao, H. Nakai, T. Vreven, J. A. Montgomery, Jr., J. E. Peralta, F. Ogliaro, M. Bearpark, J. J. Heyd, E. Brothers, K. N. Kudin, V. N. Staroverov, R. Kobayashi, J. Normand, K. Raghavachari, A. Rendell, J. C. Burant, S. S. Iyengar, J. Tomasi, M. Cossi, N. Rega, J. M. Millam, M.

- Klene, J. E. Knox, J. B. Cross, V. Bakken, C. Adamo, J. Jaramillo, R. Gomperts, R. E. Stratmann, O. Yazyev, A. J. Austin, R. Cammi, C. Pomelli, J. W. Ochterski, R. L. Martin, K. Morokuma, V. G. Zakrzewski, G. A. Voth, P. Salvador, J. J. Dannenberg, S. Dapprich, A. D. Daniels, O. Farkas, J. B. Foresman, J. V. Ortiz, J. Cioslowski, and D. J. Fox, Gaussian, Inc., Wallingford CT, 2009.
- 39 Y. Wu, X. Hao, J. Wu, J. Jin and X. Ba, *Macromolecules*, 2010, *43*, 731–738.
- 40 P. Leriche, A. Frère, A. Cravino, O. Alévêque and J. Roncali, *J. Org. Chem.*, 2007, *72*, 8332–8336.
- 41 Y. J. Cheng, S. H. Yang and C. S. Hsu, *Chem. Rev.*, 2009, *109*, 5865–5923.
- 42 J. E. House, *Inorganic Chemistry*, Academic press, Elsevier, Burlington, MA, 2008.
- 43 Y. Cui, Q. Chen, D. D. Zhang, J. Cao and B. H. Han, *J. Polym. Sci. Part A: Polym. Chem.*, 2010, *48*, 1551–1556.
- 44 B. Du, D. Fortin and P. D. Harvey, *Inorg. Chem.*, 2011, *50*, 11493–11505.
- 45 B. Ventura, A. Barbieri, F. Barigelletti, S. Diring and R. Ziessel, *Inorg. Chem.*, 2010, *49*, 8333–8346.
- 46 A. Fermi, G. Bergamini, M. Roy, M. Gingras and P. Ceroni, *J. Am. Chem. Soc.*, 2014, *136*, 6395–6400.
- 47 M. Brzezinski and T. Biela, *Macromolecules*, 2015, *48*, 2994–3004.
- 48 Z. Qu, H. Jin, Y. Guo, S. Li, H. Li, Y. Li, X. Wang and G. Yang, *J. Phys. Chem. B*, 2012, *116*, 2048–2058.
- 49 Q. Zeng, P. Cai, Z. Li, J. Qin and B. Z. Tang, *Chem. Commun.*, 2008, 1094–1096.
- 50 X. Lou, D. Ou, Q. Li and Z. Li, *Chem. Commun.*, 2012, *48*, 8462–8477.



Scheme 1 Synthetic routes of terpyridine-substituted monomer (M1).



Scheme 2 Synthetic routes of conjugated polymer (P1).

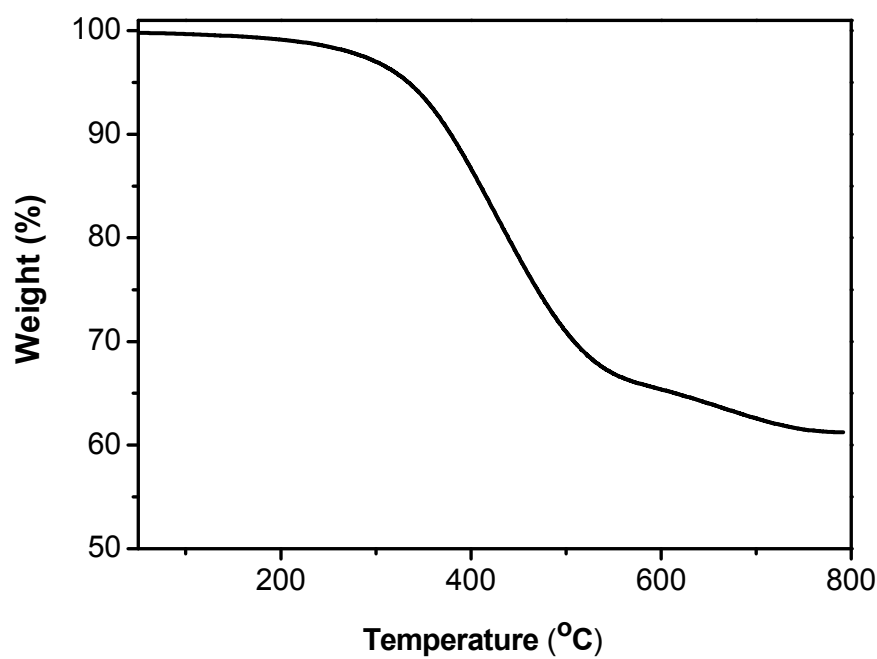


Fig. 1 TGA thermogram of **P1** at a heating rate of 20 °C min⁻¹ under nitrogen atmosphere.

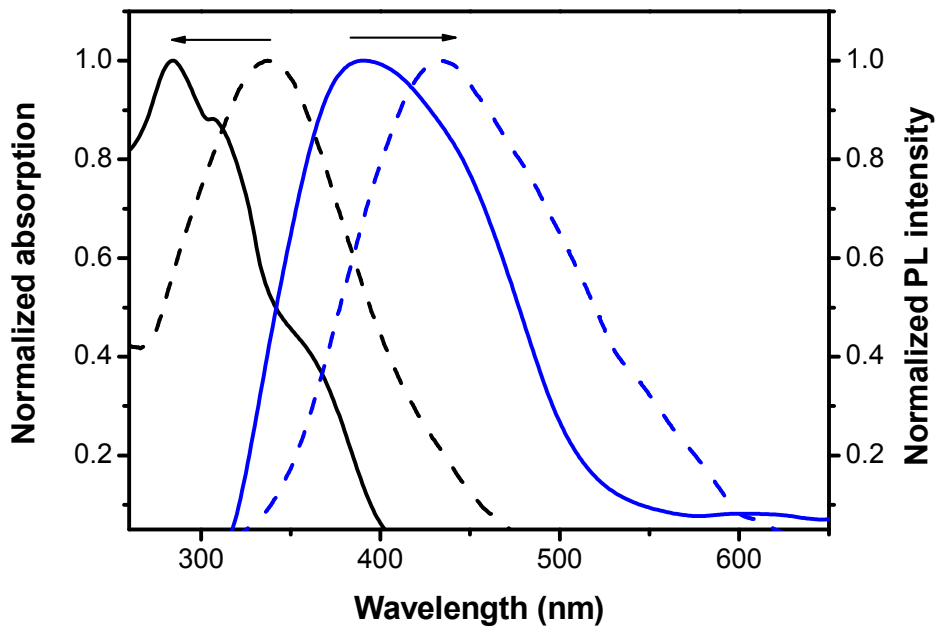


Fig. 2 Normalized UV-vis absorption and PL spectra of **P1** in THF solution (solid line) and in film (dotted line).

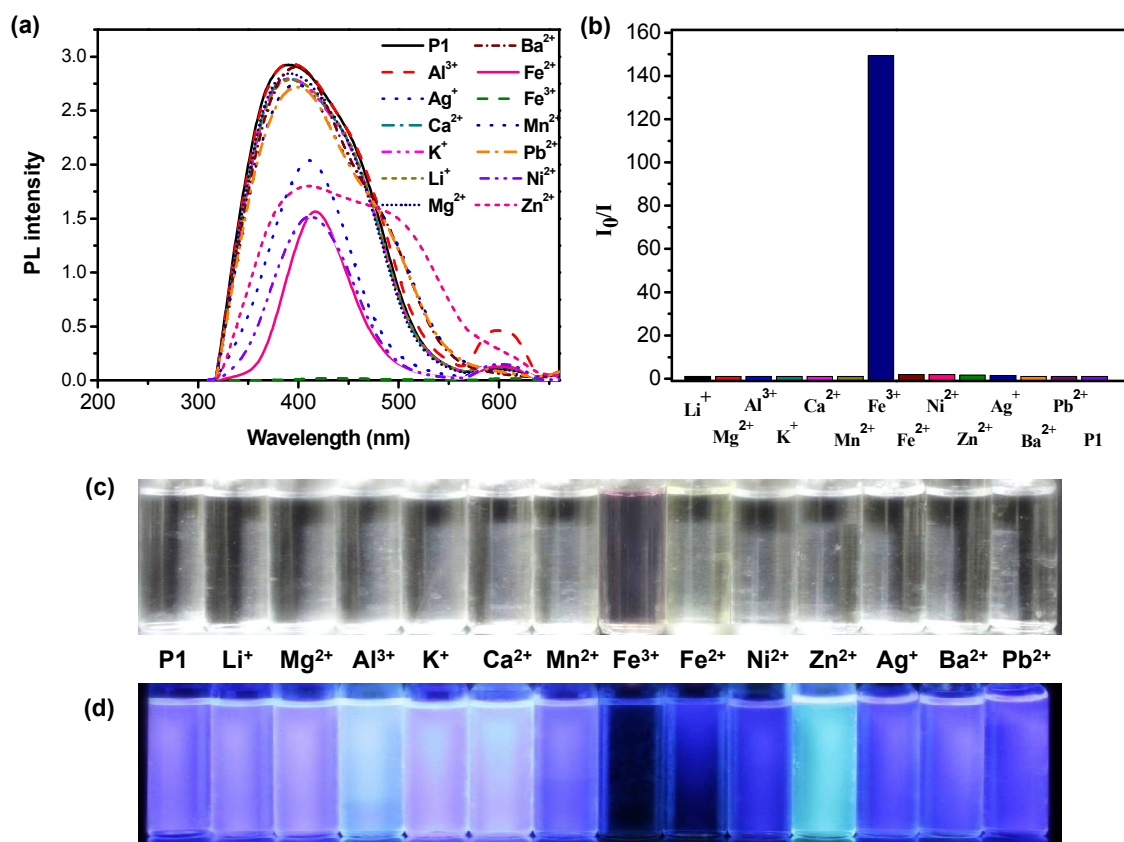


Fig. 3 (a) Photoluminescence spectra, (b) PL response profiles, and images of P1 in the presence of various cations under (c) sunlight and (d) UV excitation ($\lambda_{\text{ex}} = 300$ nm). Concentration of polymer: 1.0×10^{-6} M in THF, concentration of metal ions: 5.0×10^{-5} M.

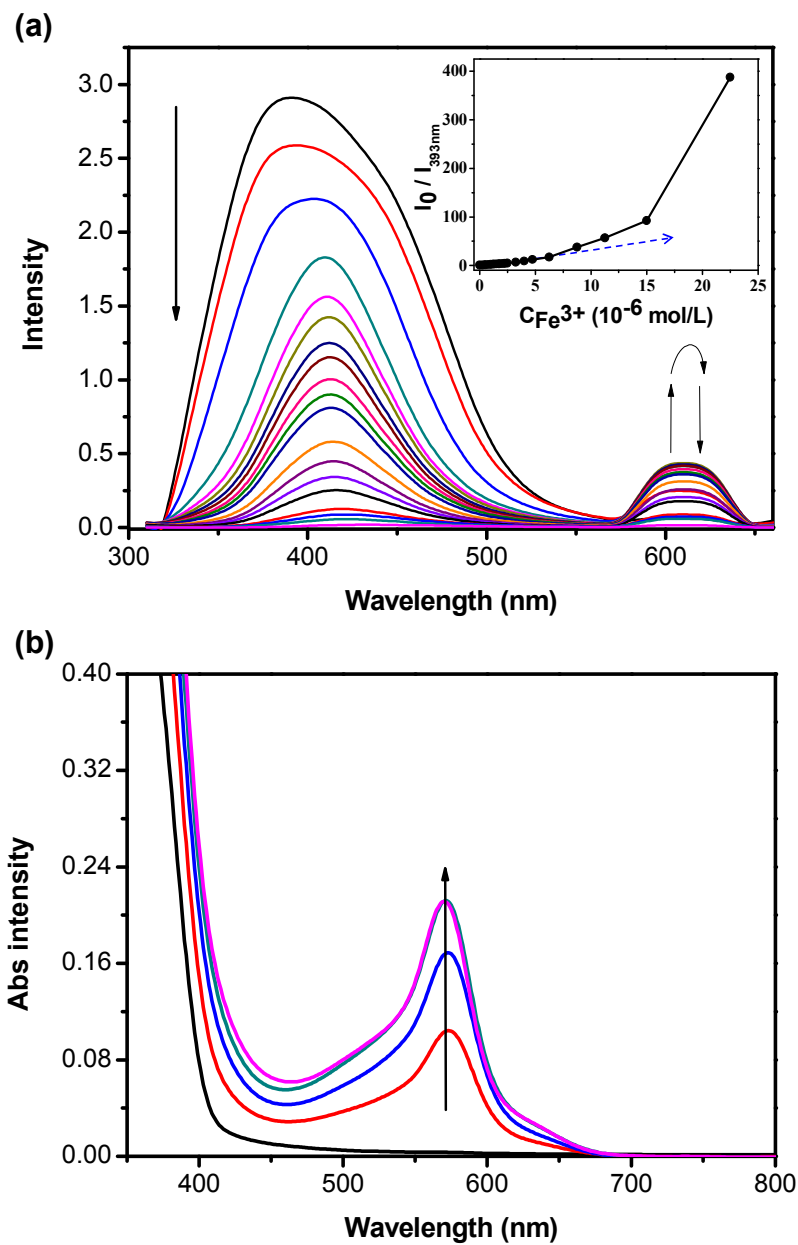


Fig. 4 (a) Photoluminescence and (b) absorption spectra of **P1** in the presence of various concentrations of Fe³⁺ ions; Inset in (a): Stern-Volmer plot of PL quenching with various concentrations of Fe³⁺ ions. Concentration of polymer: 1.0×10^{-6} M in THF.

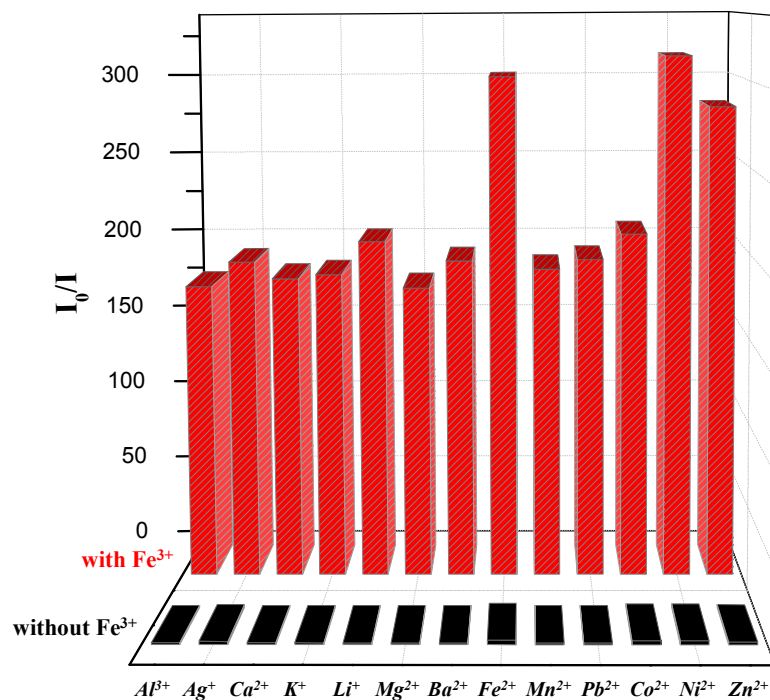


Fig. 5 Fluorescent quenching rate of **P1** in the presence of different cations with and without Fe³⁺ ions in THF solution. The black bars represent the addition of the appropriate metal ion (1.0×10^{-5} M in water) to a solution of polymer (1.0×10^{-6} M in THF). The red bars represent the subsequent addition of Fe³⁺ (1.0×10^{-5} M in water) to the former solution.

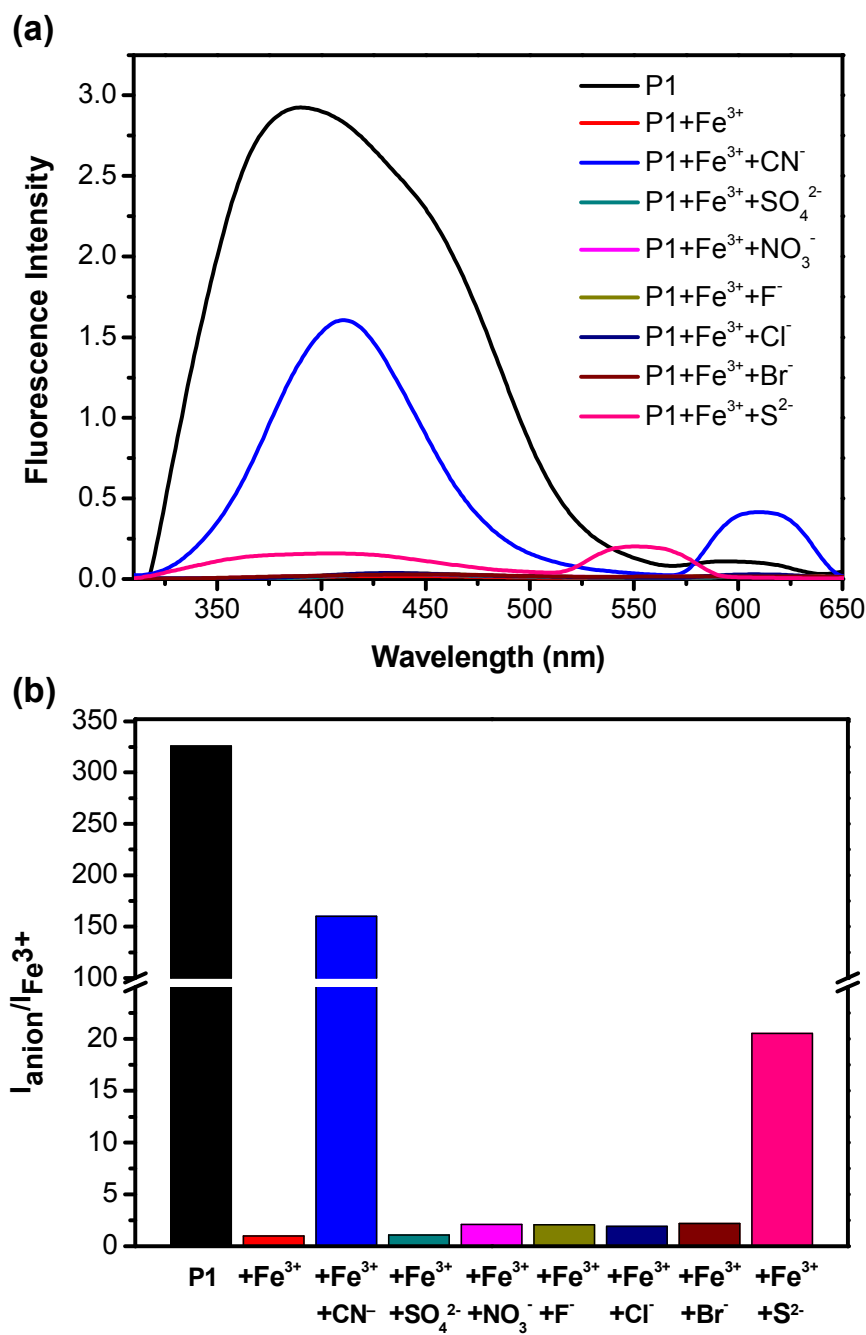


Fig. 6 (a) Photoluminescence spectra and (b) PL response profiles of **P1**– Fe^{3+} in the presence of various anions.

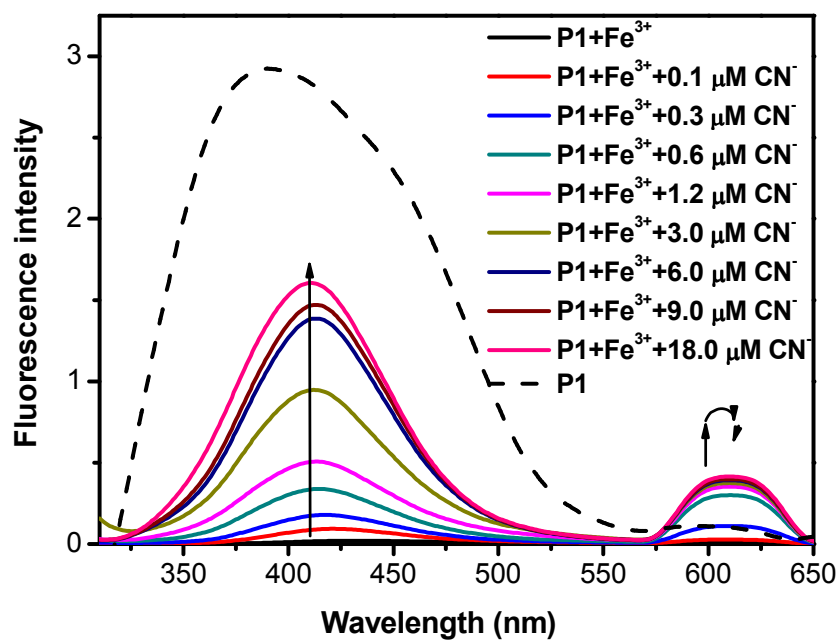


Fig. 7 Photoluminescence spectra of **P1-Fe³⁺** in the presence of various concentrations of **CN⁻** anions.

Table 1 Molecular weight and thermal properties of conjugated polymer

Polymer	Yield (%)	M_w^a ($\times 10^4$)	PDI ^a	T_g^b ($^{\circ}\text{C}$)	T_d^c ($^{\circ}\text{C}$)
P1	44.3	1.08	2.25	113.5	334.6

^a M_w and PDI of the polymer were determined by gel permeation chromatography using polystyrene standards in THF. ^b Glass transition temperatures by DSC under N_2 at a heating rate of $20^{\circ}\text{C}/\text{min}$. ^c The temperatures at 5% weight loss.

Table 2 Optical electrochemical properties of polymer

Polymer	UV-vis λ_{max}^a sol'n (nm)	UV-vis λ_{max}^a film (nm)	PL λ_{max}^b sol'n (nm)	PL λ_{max}^b film (nm)	Stokes shift ^c	Φ_{PL}^d
P1	284, 309, 363s	337	393	433	96	1.82

^a Measured in THF solution (1.0×10^{-6} M). Superscript s means the wavelength of the shoulder. ^b The excitation wavelength was 300 nm in THF for polymer. ^c Stokes shift = $\text{PL}_{(\text{film})}/\text{nm} - \text{UV}_{(\text{film})}/\text{nm}$. ^d These values of quantum yield were measured using PF as a standard (1.0×10^{-7} M, assuming a quantum yield of unity).

Table 3 Optical and electrochemical properties of polymer

Polymer	UV-vis λ_{onset}^a (nm)	$E_{\text{ox (onset)}}^b$ (V)	E_{HOMO}^c (eV)	E_{LUMO}^d (eV)	$E_{\text{g (opt)}}^e$ (eV)	$E_{\text{g (the)}}^f$ (eV)
P1	412	0.27, 0.55	-5.07, -5.35 ^g	-2.06	3.01	3.97

^a Onset wavelength of polymer in absorption spectra. ^b The cyclic voltammograms of polymer in CH₂Cl₂ (1.0 × 10⁻⁴ M) at a scanning rate of 100 mV/s (vs FOC⁺/FOC). ^c $E_{\text{HOMO}} = -(E_{\text{ox}} + 4.8)$ eV. ^d $E_{\text{LUMO}} = E_{\text{HOMO}} + E_{\text{g (opt)}}$. ^e The optical band gap was determined from the onset of absorption in CH₂Cl₂ ($E_{\text{g (opt)}} = 1240/\lambda_{\text{onset}}$). ^f The theoretical band gap was calculated using density functional theory calculations. ^g The molecular orbital was HOMO-1.